Hydroxide in pyroxene: Variations in the natural environment

Henrik Skogby,* David R. Bell, George R. Rossman

Division of Geological and Planetary Sciences, California Institute of Technology, Pasadena, California 91125, U.S.A.

Abstract

A suite of 51 pyroxenes from a wide range of geological environments was examined with infrared spectroscopy. Small amounts of OH occur in nearly all the samples, suggesting that OH groups are a minor component of most pyroxenes. The OH concentrations vary (0.002–0.12 wt% OH) as a function of geological setting with the greatest amounts occurring in mantle-derived samples. The intensities of certain OH absorption bands are somewhat correlated with pyroxene composition, in particular with the presence of trivalent cations. This suggests that crystal chemical or compositional factors also control the OH incorporation. The OH incorporated in the pyroxene structure is easily distinguishable from OH owing to amphibole lamellae, which usually occur in diopsides and often in orthopyroxenes. OH in pyroxene is probably a function of the activity of hydrous components during crystallization but may also depend on postcrystallization changes in the geological environment.

Introduction

Pyroxenes ideally are anhydrous, although in a few instances a small content of hydroxide has been identified (Wilkins and Sabine, 1973; Beran, 1976). Some of the OH is present in submicroscopic amphibole lamellae or other biopyribole lamellae, as seen in electron microscopy studies (Veblen and Buseck, 1981). Ingrin et al. (1989) showed that OH also occurs in diopsides that do not contain amphibole lamellae. The non-amphibole OH may be present on the O sites in the pyroxene structure, with cation substitutions or vacancies compensating for the charge of the H^+ ion (Beran, 1976). We have demonstrated that pyroxenes with tetrahedral Fe^{3+} are capable of incorporating H in laboratory experiments (Skogby and Rossman, 1989). However, the generality of the occurence of OH in pyroxenes has not been explored, and the relationship between OH concentration and geological provenance has not been established. There is a special interest in the study of mantle-derived pyroxenes because of the comparatively high OH content of coexisting phases (Miller et al., 1987; Aines and Rossman, 1984) and the possible effects of hydrous pyroxenes on physical properties of the mantle.

The aim of this investigation was to survey the occurrence of OH in a wide range of pyroxenes from different geological environments and to determine if there are significant natural variations in the OH content of the pyroxenes.

Experimental methods

Pyroxenes from a wide range of geological environments have been studied, including samples from metamorphic, volcanic, pegmatitic, and mantle-derived rocks. Sample types, localities, and geological environments are listed in Table 1. We examined samples ranging from essentially gem quality to turbid or altered, as well as samples with abundant inclusions.

Sample preparation consisted of orienting single crystals by morphology and interference figures, followed by cutting and doubly polishing to a typical thickness of 0.2–1.0 mm. The orientation of most samples was confirmed by IR reflectance spectroscopy. A few samples (nos. 34, 35, and 43) were available only in small amounts and could not be oriented by these methods.

Polarized spectra in the infrared region were obtained with a Nicolet 60SX Fourier transform IR spectrophotometer using a $LiIO_3$ polarizer. The three optical directions were measured on (100) and (010) sections of most samples, but (001) and a* sections were also studied for a few samples. For the orthopyroxenes, the orientation convention $\alpha = (E//b, b \sim 8.9 \text{ Å})$, $\beta = (E//a, a \sim 18 \text{ Å})$, $\gamma = (E//c, c \sim 5.2 \text{ Å})$ was used where E is the vibration direction of the incident electric vector. Unpolarized spectra were measured on the few unoriented samples (nos. 34 and 35) and on a polycrystalline sample (no. 43). A beam-path free from inclusions was carefully sought, but in some cases inclusions were impossible to avoid.

To test the influence of visible inclusions on the OH spectra, spectra were obtained from samples with both clear and included regions, which were masked to isolate each region. If the inclusions were amphibole lamellae, the OH pattern of amphiboles was readily apparent. Oth-

* Present address: Uppsala University, Institute of Geology, Department of Mineralogy and Petrology, Box 555, S-751 22 Uppsala, Sweden.

TABLE 1. Sample types, localities, and ranked OH contents for pyroxenes

Sample no.	Locality	OH abundance		Geological environment	Reference no.
		OH pfu*	Wt% OH		
47 omphacite	Roberts Victor Mine, S. Africa	0.016	0.12	eclogite xenolith in kimberlite	HRV 147 (Hatton, 1978)
20 augite	Kilbourne Hole, NM	0.014	0.10	xenolith in basalt	GRR 1656 (from S. Huebner)
30 aegirine	Caithness, Scotland	0.012	0.088	authigenic, sediment	GRR 572 (Fortey and Michie, 1978)
13 diopside**	Sydenham, Ontario	0.012	0.085	high-grade pyroxeneite	GRR 1620
17 augite	Hopi Butte, AZ	0.0095	0.073	xenocryst in mantle diatreme	GRR 1646
16 diopside	Garnet Ridge, AZ	0.0093	0.073	xenocryst in mantle diatreme	GRR 1648
7 diopside	Maui, Hawaii	0.0087	0.066	megacryst in basalt	CIT 3477
32 enstatite	India	0.0083	0.066	metamorphic	GRR 1650b
48 enstatite	Premier Mine, S. Africa	0.0061	0.050	megacryst in kimberlite	PMR 54
33 enstatite	India	0.0061	0.050	metamorphic	GRR 1650a
50 diopside	Akhmat, Soviet Union	0.0057	0.045	metamorphic?	CIT 13123
40 diopside	Elephant Butte, NM	0.0047	0.037	xenolith in basalt	GRR 1645
1 spodumene	Pala, CA	0.0043	0.041	granitic pegmatite	GRR 1659
3 diopside	Outokumpu, Finland	0.0036	0.028	metamorphic	CIT 8085
9 augite	Cedar Butte, OR	0.0035	0.027	volcanic	GRR 583
46 augite	Kangan, Andra Pradish, India	0.0032	0.026	volcanic?	GRR 1660 (from S. Huebner)
6 diopside	Binntal Vallis, Switzerland	0.0032	0.025	metamorphic	GRR 472
37 enstatite	Chichijima, Bonin Islands, Japan	0.0026	0.022	boninite lava	DB 82 (Dobson, 1986)
45 aegirine	synthetic	0.0025	0.018	synthetic, hydrothermal	GRR 264 from WA Dollase (GAW-1)
5 diopside	Mount Bity, Madagascar	0.0023	0.018	metamorphic	GRR 637
39 hedenbergite	Nordmarken, Sweden	0.0022	0.016	metamorphic	NMNH 16168
18 enstatite	Alpine, TX	0.0020	0.016	lower crustal	ALP1 (Duba et al., 1979, from S. Huebner)
12 diopside**	Sinnidal, Norway	0.0019	0.015	metamorphic	GRR 1621
8 aeg.-aug.	Magnet Cove, AR	0.0019	0.014	nepheline syenite pegmatite	CIT 349
10 diopside	Obersulzbach, Austria	0.0018	0.014	metamorphic	CIT 2593
51 augite	Juan de Fuca Ridge	0.0016	0.012	gabbroic xenolith in basalt	5-0 (Dixon et al., 1986)
19 enstatite	Kyogle, Australia	0.0014	0.011	basalt xenolith	GRR 1655 (from S. Huebner)
28 diopside	Vesuvius, Italy	0.0012	0.009	rhyolitic pumice	GRR 205 (NMNH C2429)
2 diopside	Rajasthan, India	0.0010	0.008	metamorphic	CIT 11221
38 enstatite	Zabargad, Egypt	0.0008	0.007	low-P metamorphic	GRR 649 (AMNH 49033)
21 diopside	Kauai, Hawaii	0.0007	0.006	oxidized alkali picrite	GRR 603 (Johnston and Stout, 1984)
31 enstatite**	Bamble, Norway	0.0007	0.006	megacryst	GRR 40
4 diopside	Natural Bridge, NY	0.0006	0.005	calcite vein	CIT 2135
36 enstatite**	Nain, Labrador	0.0006	0.005	megacryst, anorthosite	GRR 1616 (Veblen and Bish, 1988)
35 esseneite	Buffalo, WY	0.0005	0.004	buchite	I-90 (Foit et al., 1987)
41 diopside*	Magog, Ontario	0.0005	0.004	metamorphic	GRR 1649
14 diopside	DeKalb, NY	0.0003	0.003	metamorphic limestone	GRR 664
29 aegirine	Mount Saint Hilaire, Quebec	0.0002	0.002	nepheline syenite	CIT 8449
25 aegirine**	Magnet Cove, AR	0.0002	0.001	nepheline syenite pegmatite	CIT 11832
34 fassaite	Angra dos Reis meteorite	not detected		meteorite	GRR 290 (Keil et al., 1976)
44 diopside	synthetic	not detected		synthetic, KVO$_3$ flux	GRR 510 from J. Ito
11 hedenbergite	Harroult, Ontario	not determined†		metamorphic?	CIT 6859
15 diopside	Oka, Quebec	not determined†		metamorphic?	UCLA MS2824
22 hedenbergite**	Waldo Mine, NM	not determined†		metamorphic?	CIT 8308
23 hedenbergite**	Rio Marine, Elba, Italy	not determined†		metamorphic?	CIT 7494
24 hedenbergite**	Silver City, NM	not determined†		metamorphic?	UCLA MS2955
26 aegirine	Wausau, WI	not determined†		granitic rock	CIT 8193
27 omphacite	Möre, Norway	not determined†		eclogite	CIT 7491
42 clinoenstatite**	Chichijima, Bonin Islands, Japan	not determined†		boninite lava	MD-57 (Dobson, 1986)
43 omphacite	Burma (?)	not determined†		jade	GRR 814
49 omphacite	Roberts Victor Mine, S. Africa	not determined†		eclogite xenolith in kimberlite	390/4 (Hatton, 1978)

Note: OH concentrations were calculated using a molar absorptivity of ϵ = 150 liter/mole-cm and summed intensities for pyroxene bands in the three optical directions. NMNH = National Museum of Natural History, Smithsonian Institution. CIT = California Institute of Technology Mineral Reference Collection. AMNH = American Museum of Natural History, New York.

* Per formula unit, XYZ_2O_6.

** Visible evidence for turbidity or alteration in volume of measurement.

† OH concentration could not be determined because sample could not be oriented or was polycrystalline.

erwise, the inclusions did not contribute to the spectroscopic data, indicating that they were generally anhydrous phases.

The OH concentrations in the samples were calculated from the intensities of the OH bands according to Beer's law: Absorbance = ϵ × path length × OH concentration. The molar absorptivity (ϵ) was estimated by a number of methods described in the results section, assuming the

TABLE 2. Structural formulae of pyroxenes analyzed by electron microprobe

	1 sp	2 di	3 di	4 di	5 di	6 di	7 di	8 ae-aug	9 aug	10 di	12 di	13 di	14 di
Si	1.992	2.006	1.990	1.961	1.981	1.979	1.731	1.986	1.884	1.994	1.997	1.981	2.012
[4]Al	0.008	0.000	0.010	0.039	0.007	0.021	0.269	0.014	0.116	0.006	0.003	0.019	0.000
[6]Al	0.997	0.016	0.023	0.017	0.000	0.007	0.096	0.017	0.048	0.019	0.052	0.027	0.013
Ti	0.000	0.000	0.000	0.003	0.000	0.000	0.047	0.014	0.026	0.000	0.002	0.001	0.000
Fe^{3+}	0.000	0.000	0.000	0.044	0.043	0.054	0.122	0.622	0.027	0.040	0.036	0.068	0.000
Cr	0.000	0.000	0.019	0.000	0.000	0.000	0.008	0.001	0.015	0.000	0.001	0.001	0.000
Mg	0.000	0.916	0.861	0.746	0.908	0.799	0.720	0.182	0.875	0.713	0.824	0.485	0.970
Fe^{2+}	0.001	0.069	0.089	0.171	0.040	0.107	0.106	0.120	0.171	0.213	0.126	0.413	0.016
Mn	0.000	0.002	0.002	0.004	0.003	0.006	0.004	0.012	0.004	0.021	0.001	0.025	0.000
Ca	0.001	0.971	0.976	0.987	1.009	0.989	0.846	0.377	0.810	0.941	0.867	0.900	0.971
Na	0.005	0.020	0.030	0.028	0.009	0.038	0.051	0.655	0.024	0.053	0.091	0.080	0.017

	28 di	29 ae	30 ae	31 en	32 en	33 en	34** fas	35 ess	36† en	37 en	38 en	39 hd	40 di
Si	1.801	2.007	1.995	2.004	2.001	1.999	1.728	1.360	1.93	1.984	1.976	1.980	1.926
[4]Al	0.199	0.000	0.000	0.000	0.000	0.001	0.272	0.636	0.07	0.016	0.024	0.006	0.074
[6]Al	0.069	0.041	0.000	0.004	0.032	0.017	0.161	0.000	0.04	0.000	0.017	0.000	0.007
Ti	0.032	0.010	0.000	0.000	0.002	0.000	0.059	0.029	0.00	0.001	0.001	0.000	0.014
Fe^{3+}	0.081	0.804	0.980	0.000	0.000	0.000	0.000	0.605	0.00	0.008	0.005	0.041	0.039
Cr	0.002	0.000	0.001	0.001	0.000	0.000	0.005	0.000	0.01	0.009	0.001	0.000	0.014
Mg	0.739	0.016	0.003	1.698	1.525	1.730	0.568	0.339	1.49	1.718	1.975	0.416	0.954
Fe^{2+}	0.123	0.073	0.000	0.283	0.417	0.238	0.223	0.026	0.45	0.222	0.000	0.502	0.066
Mn	0.004	0.028	0.000	0.000	0.008	0.005	0.002	0.004	0.01	0.004	0.000	0.064	0.003
Ca	0.933	0.142	0.001	0.010	0.015	0.009	0.968	0.982	0.01	0.038	0.000	0.984	0.889
Na	0.018	0.878	1.019	0.000	0.000	0.000	0.002	0.017	0.00	0.000	0.001	0.007	0.014

Note: The formulae are normalized to four cations.
* 18, 19, and 20: Analyses provided by J.S. Huebner.
** 34: Analysis from Hazen and Finger (1977).
† 36: Analysis from Veblen and Bish (1988).
‡ 0.011 K also present in sample.

species OH expressed in mol/L. Absorbances were calculated by summing the peak height in the three optical directions for all peaks assumed to be caused by intrinsic (pyroxene) OH as

$$\text{Abs}_{sum} = \sum_{i=1}^{n} (\text{Abs}_i(\alpha) + \text{Abs}_i(\beta) + \text{Abs}_i(\gamma)).$$

For a few samples where spectra in all three optical directions could not be obtained, the OH concentration was estimated by comparison with spectra of other samples.

The samples were analyzed with a JEOL 733 electron microprobe at 15 kV accelerating potential and 15 nA Faraday cup current. Data were corrected as described in Skogby and Rossman (1989). Structural formulas of the samples normalized to four cations are in Table 2.

RESULTS

IR spectroscopy

Narrow absorption bands occur in the 3000–3700 cm^{-1} region of the infrared spectra of nearly all samples. Both OH and H_2O absorb in this region. In nearly all cases, the absence of a water combination band near 5200 cm^{-1} indicates that the absorbing species is hydroxide ion. The only exceptions were altered or fibrous samples that showed evidence of the much broader band of liquid H_2O. The OH$^-$ ion is present in all our natural samples, except the meteoritic fassaite (no. 34). The spectroscopic features (band position, intensity, polarization) vary among samples depending on composition, geologic environment, and locality. The polarized spectra obtained on oriented sections show that all bands are pleochroic, which means that the OH dipoles giving rise to these bands are crystallographically oriented.

For purposes of classification, the OH$^-$ absorption bands in pyroxenes have been divided into two classes (Skogby and Rossman, 1989). The first class occurs at higher wavenumbers (approximately 3675 cm^{-1}) in the spectra of many pyroxenes and resembles the sharp peaks in amphibole spectra. These bands, referred to here as amphibole bands, are most prominent in the spectra of somewhat altered pyroxenes and in samples with visible amphibole lamellae. They are weaker or absent in gem-quality pyroxenes. The second class occurs at lower wavenumbers in the spectra of all hydrous pyroxenes, consisting of broader absorptions, which we call pyroxene bands. They are also present in the spectra of gem-quality samples and are not associated with foreign phases.

The pyroxene bands occur between 3000–3640 cm^{-1} and for clinopyroxenes can be further divided into two groups, based on pleochroic behavior (Table 3). Three bands may occur around 3350, 3450, and 3525 cm^{-1} and have the pleochroism $\gamma > \alpha = \beta$. Another band is usually present at 3620–3640 cm^{-1} with $\alpha = \beta$, $\gamma = 0$. For different samples there is a large range of absorption intensities per unit thickness, suggesting large variations in OH concentration.

TABLE 2—*Continued*

16 di	17 aug	18* en	19* en	20* aug	21 di	25 ae
1.983	1.841	1.815	1.915	1.776	1.710	2.002
0.017	0.159	0.185	0.085	0.224	0.228	0.000
0.109	0.084	0.089	0.068	0.160	0.049	0.025
0.001	0.039	0.014	0.004	0.041	0.062	0.030
0.007	0.054	0.075	0.000	0.072	0.245	0.760
0.063	0.008	0.001	0.009	0.000	0.000	0.001
0.807	0.824	1.367	1.538	0.732	0.748	0.053
0.037	0.131	0.380	0.305	0.155	0.013	0.111
0.002	0.003	0.006	0.004	0.003	0.004	0.015
0.810	0.792	0.058	0.062	0.745	0.882	0.152
0.164	0.065	0.010	0.010	0.092	0.059	0.851

41 di	43 omp	45 ae	47‡ omp	48 en	50 di	51 aug
1.967	2.005	1.976	1.969	1.977	2.012	1.927
0.007	0.000	0.015	0.031	0.023	0.000	0.073
0.000	0.567	0.000	0.558	0.014	0.011	0.031
0.001	0.006	0.001	0.008	0.007	0.002	0.015
0.060	0.000	0.978	0.000	0.003	0.000	
0.001	0.000	0.001	0.002	0.003	0.019	0.008
0.776	0.407	0.002	0.425	1.734	0.947	0.951
0.152	0.032	0.000	0.058	0.191	0.032	0.187
0.014	0.003	0.000	0.001	0.004	0.002	0.006
1.020	0.396	0.000	0.478	0.033	0.950	0.798
0.003	0.583	1.026	0.459	0.011	0.025	0.016

Fig. 1. Polarized IR spectra (α, β, γ) of diopside from India (no. 2). Spectra normalized to 1 mm thickness. Note weak amphibole band at 3675 cm⁻¹; other bands are referred to as pyroxene bands.

Diopside-hedenbergite

Diopside spectra usually have four pyroxene bands (Fig. 1). Three bands occur close to 3355, 3460, and 3535 cm⁻¹ in most samples, with the pleochroism $\gamma > \alpha = \beta$. A fourth band occurs at 3645 cm⁻¹ with $\alpha = \beta$ and $\gamma = 0$. The band at 3460 cm⁻¹ is usually the strongest in the spectrum. The position and pleochroism of the absorption bands are similar for different samples, but the absolute intensities vary strongly (Fig. 2). Bands that are attributed to amphibole are present in the spectra of most diopsides. Spectra obtained from a synthetic diopside grown by J. Ito from a KVO_3 flux (no. 44) show neither pyroxene nor amphibole absorption bands, demonstrating that these bands arise from something other than the lattice vibrations of pyroxene itself.
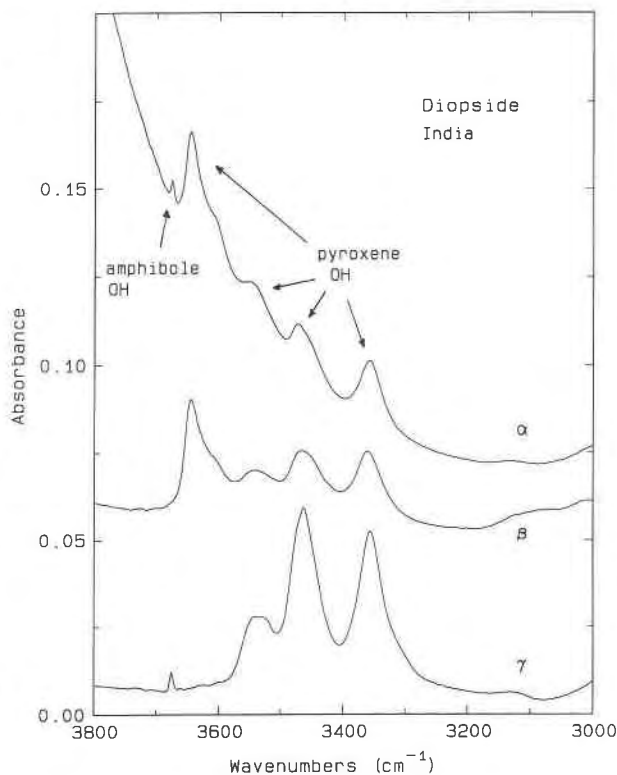
Hedenbergite spectra are similar to diopside spectra, with two absorption bands at 3440 and 3520 cm⁻¹ and a weak 3640 cm⁻¹ band. Some spectra have several sharp amphibole peaks, resembling spectra of amphiboles of intermediate actinolite-grunerite compositions (Burns and Strens, 1966). A broad band at 3200–3700 cm⁻¹ caused by molecular water occurs in the spectra of some altered hedenbergites.

Augite

Three pyroxene bands are usually present in augite spectra (Fig. 3). Two occur at 3465 and 3520 cm⁻¹ with

TABLE 3. General properties of pyroxene absorption bands

Sample	Wavenumber [cm⁻¹]			
	3620–3640	3520–3535	3450–3465	3350–3355
Diopside	$\alpha = \beta$, $\gamma = 0$	$\gamma > \alpha = \beta$	$\gamma > \alpha = \beta$	$\gamma > \alpha = \beta$
Hedenbergite	$\alpha = \beta$, $\gamma = 0$	$\gamma > \alpha = \beta$	$\gamma > \alpha = \beta$	—
Augite	$\alpha = \beta$, $\gamma = 0$	$\gamma > \alpha = \beta$	$\gamma > \alpha = \beta$	—
Aegirine-augite	$\alpha > \beta > \gamma$	—	—	—
Compositional association	M^{3+}	Fe^{2+}	Fe^{2+}, Mg	Mg
Thermal stability*	most stable	unstable	stable	unstable
Reequilibration**	increase	decrease	increase	decrease

* Thermal stability refers to heating experiments performed on diopsides and aegirine-augite in air or H_2 at one atmosphere pressure (Skogby and Rossman, 1989).
** Reequilibration refers to hydrothermal experiments performed on diopsides at 600–800 °C and 1–2 kbar pressure.
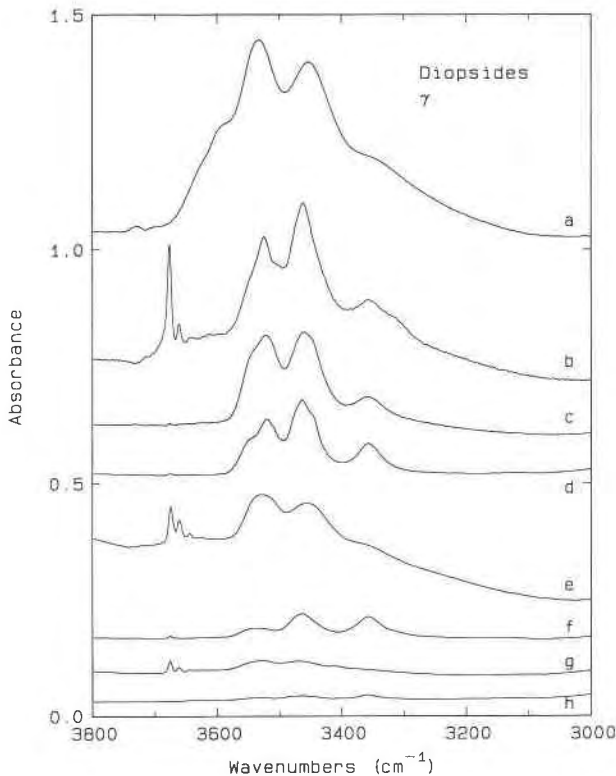
Fig. 2. IR spectra of diopsides in γ-polarization plotted for 1 mm thickness, (a) no. 16, Garnet Ridge, AZ, (b) no. 3, Outokumpu, Finland, (c) no. 6, Binntal Vallis, Switzerland, (d) no. 5, Mount Bity, Madagascar, (e) no. 12, Sinnidal, Norway, (f) no. 2, Rajasthan, India, (g) no. 4, Natural Bridge, NY, (h) no. 14, DeKalb, NY.

Fig. 3. Polarized spectra of augite (no. 17, Hopi Butte) normalized to 1 mm thickness.

the pleochroism $\gamma > \alpha = \beta$, and a third band, usually the strongest, occurs at 3635 cm^{-1} with $\alpha = \beta$, $\gamma = 0$. In contrast to diopside, there is no band around 3355 cm^{-1}. The absorption bands in augite spectra are usually broader than in diopside spectra. Amphibole bands have not been detected in augite spectra.

Aegirine and aegirine-augite

Two absorption bands may occur in the spectra of aegirine and aegirine-augite: one band at 3620–3650 cm^{-1} (Fig. 4), and another band which is sometimes present around 3550 cm^{-1}. In contrast to the 3630–3640 cm^{-1} band in augite and diopside, the corresponding band in aegirine has an absorption component in the γ direction. This may be caused by the γ and α directions having different angles, with the c axis in the (010) plane in aegirines and diopside-augites. Spectra of an authigenic aegirine sample of almost exact end-member composition (Fortey and Michie, 1978) have a strong band at 3555 cm^{-1} in all the three optical directions. Spectra of a synthetic aegirine sample (no. 45) provided by W. A. Dollase and grown by hydrothermal methods have rather sharp bands at 3675 cm^{-1} (probably amphibole), 3620 cm^{-1}, 3555 cm^{-1}, and 3485 cm^{-1} in its spectrum.

Omphacite

Only one well-oriented omphacite sample has been studied. Its spectrum (Fig. 5) is similar to spectra of pyroxenes in the diopside-hedenbergite series, but the absorption bands are considerably stronger. Bands occur at the same wavenumbers in spectra of two other unoriented omphacites. No amphibole bands were detected in any of the omphacite samples.

Orthopyroxene

Orthopyroxene spectra differ from clinopyroxene spectra. Prominent bands may occur at 3410, 3510, and 3560 cm^{-1} and are often sharper than clinopyroxene bands (Fig. 6). The pyroxene bands have the pleochroism $\gamma > \alpha \sim \beta$. Amphibole bands occur in some samples, with the strongest absorbance in the β direction. The spectra of two anorthosite megacryst samples (Labrador and Bamble) are dominated by a strong amphibole band around 3660 cm^{-1} in the β direction (but which are weak in the γ direction in Fig. 6). Both of these samples are known from electron microscopy studies to contain thin lamellae of clinoamphibole (Veblen and Bish, 1988).

Disordered pyribole and jimthompsonite

Electron microscopy studies have shown that pyroxenes may contain not only submicroscopic amphibole lamellae but also disordered pyribole and the triple-chain
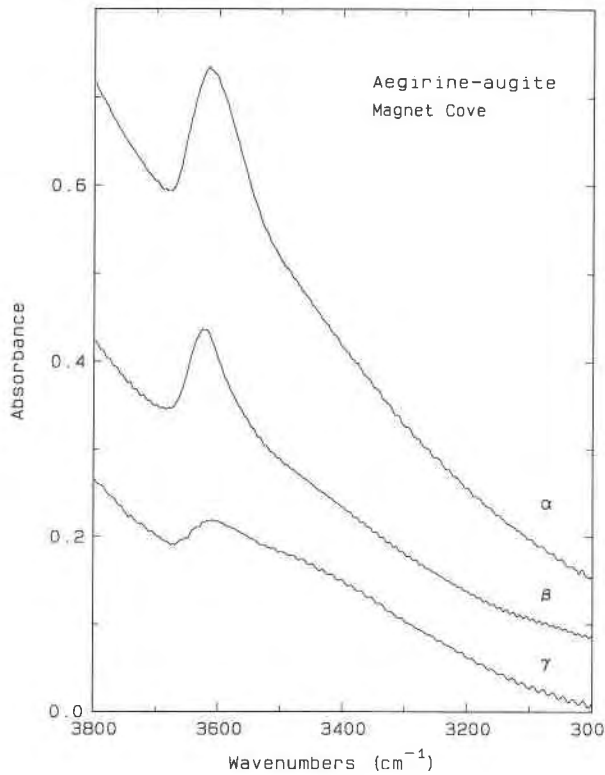
Fig. 4. Polarized spectra of aegirine-augite (no. 18, Magnet Cove) normalized to 1 mm thickness.
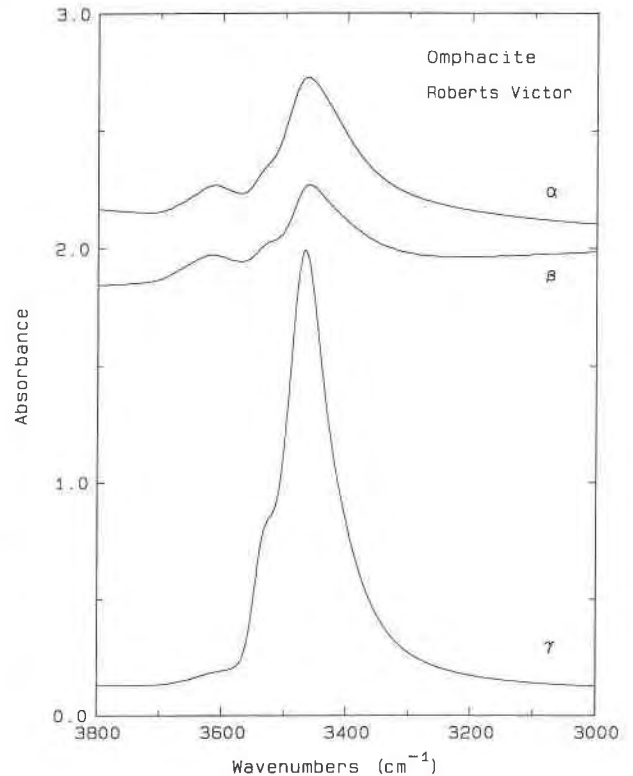

Fig. 5. Polarized spectra of omphacite (no. 47, Roberts Victor, South Africa) normalized to 1 mm thickness.

analogue of amphibole, jimthompsonite (Veblen and Buseck, 1981). The IR patterns of these phases are not known, and the possibility exists that they cause some of the OH bands in pyroxene spectra. To resolve this uncertainty, we measured IR spectra of a jimthompsonite sample provided by J. L. Rosenfeld. Spectra of both jimthompsonite and anthophyllite were obtained on a thin section using unpolarized light and microscope spectroscopic methods. The phases were identified by their typical cleavage angles of 38° for jimthompsonite and 55° for anthophyllite. The spectrum of jimthompsonite is very similar to that of anthophyllite, with sharp bands occurring around 3660 cm^{-1} (Fig. 7). Because the structural environment about OH in the disordered pyriboles and jimthompsonite are similar, we are confident that the pyroxene bands are not caused by jimthompsonite or related disordered pyriboles.

OH concentration

IR spectroscopy provides a very sensitive method for detecting trace amounts of OH in minerals but is not intrinsically self-calibrating. In order to calibrate the spectroscopy data, an independent method of water analysis is required. Wilkins and Sabine (1973) measured H_2O concentrations in diopside from Tyrol, Austria, by dehydration and P_2O_5 coloumetry, and presented an unpolarized spectrum obtained on a (110) section. To compare these data to our polarized spectra, we measured

unpolarized spectra on (110) sections of two diopsides (India and Ural) that have OH patterns similar to the Tyrol sample. The resulting OH concentrations and molar absorptivities are in Table 4. The most OH-rich pyroxenes have OH contents approaching those of some mantle-derived amphiboles (e.g., kaersutite B-CH-5-A; Boettcher and O'Neil, 1980).

We also tried a number of other methods to calibrate the pyroxene OH bands: A nuclear profiling method (Rossman et al., 1988) was used to determine the OH content in three of the pyroxene samples (Table 4). Molar absorptivities for some hydrous minerals (amphiboles, micas, and tourmaline; Skogby and Rossman, in preparation) with stoichiometric OH contents were determined and applied to the pyroxene data. The calibration of Paterson (1982), derived primarily from glasses using inte-

TABLE 4. Estimated molar absorptivities

No. sample	Wt% OH	Abs/mm	ϵOH
50 diopside, Ural*	0.047	1.37	164
2 diopside, India*	0.010	0.24	138
20 augite, Kilbourne Hole**	0.102	2.86	151
48 enstatite, Premier**	0.096	1.31	70

Note: ϵ-values were calculated assuming the species OH according to absorbance = ϵ × path × concentration, where path is in cm and concentration is in mol/L.
* OH estimated by comparison with data of Wilkins and Sabine (1973).
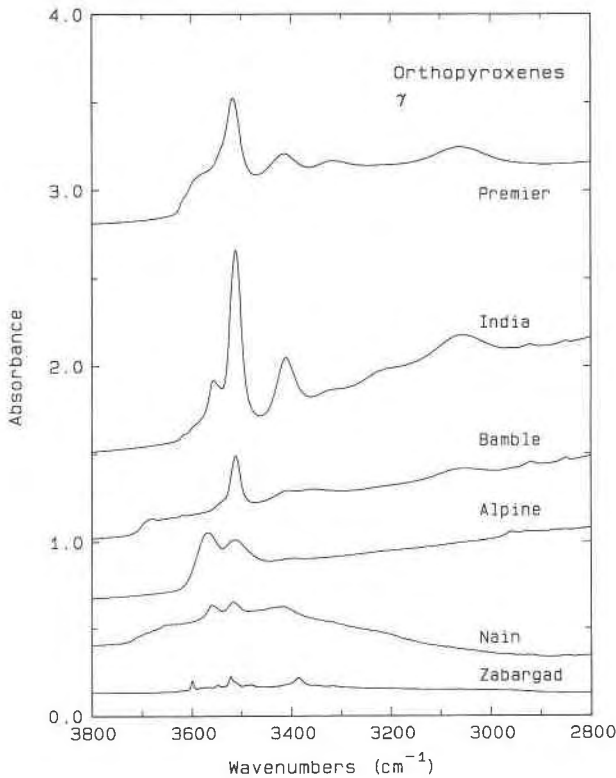** Water content determined by R. Livi using nuclear profiling analysis.

Fig. 6.   Spectra of orthopyroxenes in γ-polarization plotted for 1 mm thickness. From top to bottom: no. 22, Premier Mine; no. 32, India; no. 18, Bamble; no. 18, Alpine; no. 20, Nain; no. 21, Zabargad. Amphibole bands occur in the β spectra of the samples from Nain, India, and Bamble.
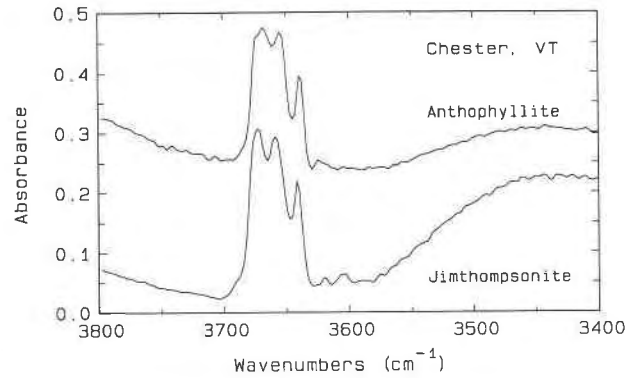

Fig. 7.   Unpolarized spectra of coexisting anthophyllite (top) and jimthompsonite (bottom). Spectra were obtained from a thin-section cut perpendicular to the c axis. Sample thickness 30 μm. The broad band centered around 3400 cm⁻¹ is due to the glue in the thin section and does not represent sample absorption. Band positions for the jimthompsonite are 3672, 3657, and 3641 cm⁻¹.

grated molar absorptivities, was also tried. The OH concentrations obtained from the different calibration methods show considerable scatter, but most methods give values within a factor of two of the calculation of Wilkins and Sabine's data. For purposes of estimating the OH contents and variation among samples (Table 1), we used $\epsilon = 150$ mol⁻¹ cm⁻¹. As better calibrations are established, the values in Table 1 may need revision.

Discussion

In assessing the OH content of pyroxenes, it is convenient to think in terms of two types of controlling factors. These may be broadly classed as external and internal in character. The internal controls are structural limitations imposed by crystal chemistry and refer to the degree to which pyroxene of a particular composition can accommodate OH. External controls are factors such as f_{H_2O}, f_{H_2}, a_{OH^-}, or other characteristics of the petrological environment that may result in pyroxene of a given composition having varying OH amounts. It is not easy to establish which factor exerts the dominant influence, since the internal and external parameters are often correlated. In the following discussion we attempt to evaluate the relative roles of these factors in producing the OH variability in our sample set.

External factors

The OH concentrations of pyroxenes vary significantly from one geological environment to another (Table 1). Although much scatter in OH concentration exists in samples of similar paragenesis, several useful observations can be made from the broad trends displayed. It is encouraging to note that the weakest OH spectra are from anhydrous environments, namely the meteoritic and flux-grown synthetic samples. This is circumstantial evidence that OH in pyroxenes reflects some aspect of volatile activity in the geological environment and is not influenced by superficial processes such as atmospheric contamination. There is a general tendency for the samples from higher pressure environments to contain higher concentrations of OH. Thus, crustal pyroxenes from metamorphic environments are highly variable in OH content (0.003–0.085 wt% OH), with the greatest amounts occurring in samples from high-grade rocks. This is taken to the extreme in mantle-derived materials, which are consistently among the most hydrous of our samples. The most hydrous pyroxene is an omphacite from an eclogite xenolith in kimberlite of the Roberts Victor Mine, South Africa. This sample, with 0.12 wt% OH, has, by analogy with other Roberts Victor eclogites, an estimated pressure of origin in the range 35–55 kbar (Hatton, 1978; Basu et al., 1986). It seems unlikely that all these high-pressure pyroxenes have crystallized in water-rich environments. We therefore suspect that their OH-rich characteristics could be linked to an internal aspect associated with the high-pressure environment, for example, their more aluminous nature.

Ingrin et al. (1989) and Skogby and Rossman (1989) have shown that OH may be rapidly removed and then reintroduced into pyroxenes by heating and hydrothermal treatment at low pressures. It may be important to note that all our mantle pyroxenes (which are uniformly

OH-rich) were found as xenoliths or xenocrysts erupted in alkaline volcanic rocks. These host magmas are typically volatile-rich, and the OH content of the included pyroxenes may be influenced during their transport to the surface. It might be instructive to compare the OH content of xenolithic pyroxenes of both crustal and mantle origin in such eruptives.

Pyroxenes from crustal volcanic and plutonic igneous rocks are also highly variable in OH content. Spodumene from a granitic pegmatite (no. 1) and an enstatite (no. 37) phenocryst that crystallized at about 2 kbar from a hydrous boninite magma (Dobson, 1986) both contain appreciable OH contents, 0.04 and 0.02 wt%, respectively. Pyroxenes from syenitic rocks (nos. 8, 25, and 29), anorthosite (no. 36) and a rhyolite (no. 28) are poorer in OH. One of the most OH-rich samples is an aegirine of essentially end-member composition (no. 30), believed to be of sedimentary authigenic or diagenetic origin (Fortey and Michie, 1978). The high OH content of this sample shows that such concentrations are not restricted to pyroxenes from high-pressure environments (at least not in aegirines). The presence of coexisting pyrite suggests relatively reducing conditions in the sediment. Pyroxenes that have formed in anomalously oxidizing environments (buchite and oxidized alkali picrite, sample nos. 35 and 21, respectively) are very poor in OH, suggesting that f_{O_2} may also play a role.

Consideration of the above geologic factors leads us to suggest that the OH content of pyroxenes is some function of the activity of hydrous species. After crystal growth, changes in the f_{O_2} and f_{H_2} may affect the final OH concentration. Complicating this relationship are crystal chemistry effects that modify the proportionality between pyroxene OH content and external f_{H_2O} (i.e., activity coefficient of the hydropyroxene component).

Internal factors

The relatively high OH concentrations detected (up to 0.016 OH per formula unit) suggest that the incorporation of H is associated with, and its charge balanced by, the minor elements (e.g., Al, Cr, Fe^{3+}, Na) or vacancies, rather than by trace elements that are unlikely to be present in adequate amounts. Since the OH band positions and relative intensities of the OH-poor samples closely match those of OH-rich samples, the substitutional mechanisms are likely to be the same.

The IR patterns obtained for the different types of clinopyroxenes show clear compositional dependence. Spectra of aegirine-augites are dominated by the 3620–3640 cm^{-1} band (Fig. 4), whereas spectra of Al-poor diopsides are dominated by the bands around 3450, 3525, and 3350 cm^{-1} (Fig. 1). Augite spectra have a more even intensity distribution between the two groups of bands (Fig. 3).

The correlation between chemical composition and OH-band intensity was systematically examined, including correlations among OH-band intensities and the concentration of single elements and sets of elements. A few
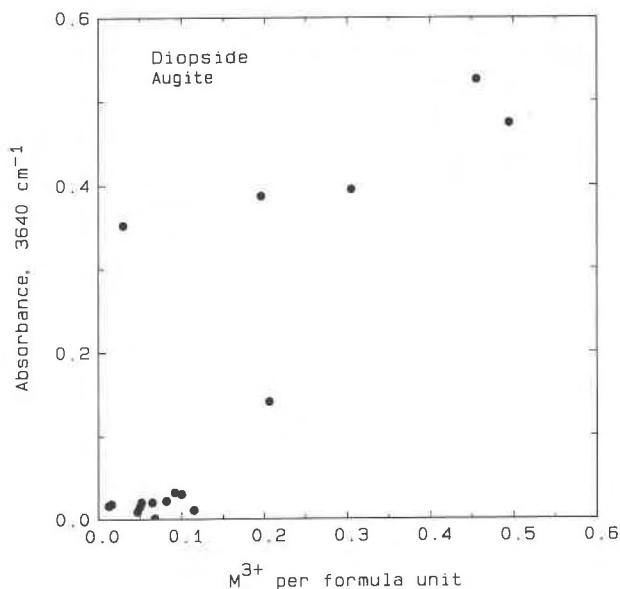

Fig. 8. Summed absorbance per mm thickness in the three optical directions of the band at 3620–3640 cm^{-1} plotted versus Al + Cr + Fe^{3+} per formula unit. Data represent diopside-hedenbergites, augites, and aegirine-augites.

correlations were found for clinopyroxenes, but no correlations were found for the less chemically variable orthopyroxenes.

The correlation between the summed absorbance intensity of the 3620 to 3640 cm^{-1} bands in the three optical directions and the sum of trivalent ions (mostly Al) for diopsides-hedenbergites and augites is displayed in Figure 8. The weak correlation found might be due to a spatial association of the OH causing this band with trivalent ions. Alternatively, the geochemical environment in which high-Al pyroxenes grows might favor incorporation of OH in the pyroxene structure. The clustering of samples close to the origin indicates that Al-poor samples seldom have strong 3640 cm^{-1} bands. For Fe^{3+}-rich samples, this band shifts towards 3620 cm^{-1}.

Figure 9 shows the sum of the intensities of the two bands occurring around 3525 and 3450 cm^{-1} versus the Fe^{2+} concentration for crustal diopsides-hedenbergites. The somewhat triangular-shaped distribution (no samples plot in the upper left corner) suggests that Fe^{2+}-rich samples can accommodate more OH than Fe^{2+}-poor samples. The samples with high Fe^{2+} contents and low OH concentration may have formed under conditions unfavorable for OH incorporation (e.g., low f_{H_2O} and f_{H_2}).

The band at 3350 cm^{-1} seems to be connected with Mg; it occurs only in spectra of diopsides with Mg/(Mg + Fe) > 0.80. The intensity of the band relative to the other bands increases with increasing Mg content.

The variable OH saturation of pyroxenes caused by equilibration in different geological environments is likely to obscure possible correlations such as those investigated above. In order to reduce this source of variability,
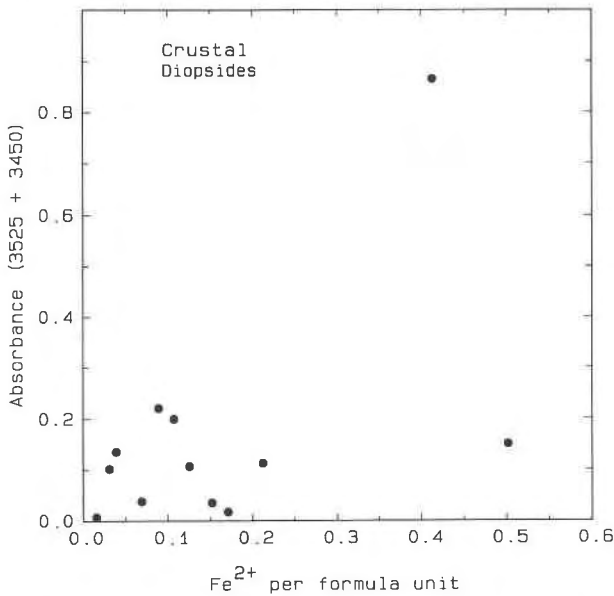
Fig. 9. Summed absorbance per mm thickness in the three optical directions of the bands at 3525 and 3450 cm^{-1} plotted versus Fe^{2+} per formula unit. Data represent crustal diopsides and hedenbergites.
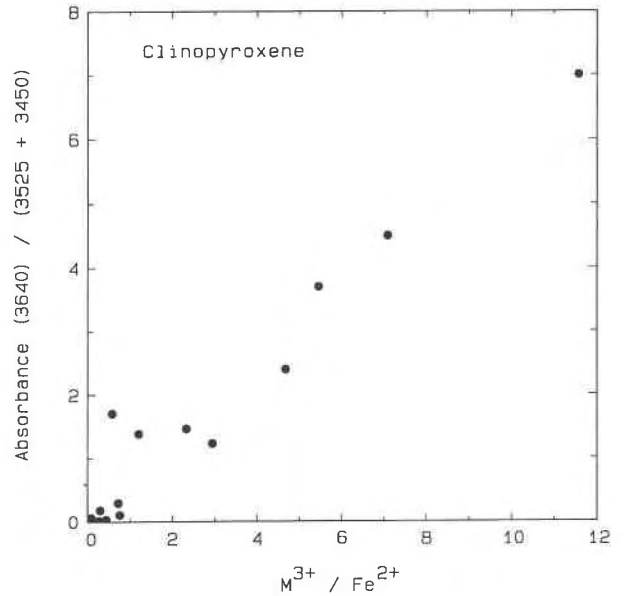

Fig. 10. Ratio of summed absorbance for the bands around 3450 and 3525 cm^{-1} plotted versus the ratio (Al + Cr + Fe^{3+})/Fe^{2+}. Data represent hedenbergites, augites, aegirine-augites, and diopsides with Fe >0.10 per formula unit.

we examined the correlation between the ratio of individual band intensities and the ratio of the cation concentrations with which the bands appear to be associated. In Figure 10, the ratio (Al + Cr + Fe^{3+})/Fe^{2+} is plotted versus the ratio (Abs$_{3620-3640}$/(Abs$_{3525}$ + Abs$_{3450}$) for diopside-hedenbergites, augites, and aegirine-augites. Diopsides with Fe < 0.10 per formula unit were excluded from the plot because of the large error in (Al + Cr + Fe^{3+})/Fe^{2+} for the Fe-poor samples. The correlation of the ratios is consistent with a correlation of trivalent ions with the band in the 3620 to 3640 cm^{-1} region, and a correlation of Fe^{2+} with the bands at 3450 and 3525 cm^{-1}, independent of total OH concentration.

The correlations between composition and absorbance intensities are in Table 3. Also listed are the thermal stability and reequilibration behavior of the OH ions giving rise to the bands (Skogby and Rossman, 1989). These pyroxene bands can be divided into two groups: one occurring at 3620 to 3640 cm^{-1} associated with trivalent ions, having the pleochroism $\alpha = \beta$, $\gamma = 0$, and a relatively stable thermal behavior. The second group consists of the three bands around 3525, 3460, and 3350 cm^{-1} associated with divalent ions, having the pleochroism $\gamma > \alpha = \beta$ and a more complex thermal behavior.

The distribution of OH band intensity in omphacite is especially interesting because the structure can be regarded as a solid solution of jadeite and diopside. As seen from the omphacite spectra (Fig. 5), the bands at 3525 and 3460 cm^{-1} dominate the spectra, suggesting that OH preferably enters the diopside environment.

OH orientation

The pleochroic behavior of the OH bands in spectra of the Indian diopside is summarized in Table 5. The pyroxene band at 3645 cm^{-1} is due to dipoles inclined to the (001) plane, closer to the b axis than the a axis, which is in agreement with the findings of Beran (1976), who suggested that the OH dipole was present in the O(2) position pointing towards O(3). The O(2) position is the most favorable for OH substitution, since it is highly underbonded (Cameron and Papike, 1980). If Al substitutes for Si, it will increase the underbonded character of the O(2) even further, making OH substitution at the O(2) site more favorable. However, the intensity of the 3645 cm^{-1} band correlates better with total Al than tetrahedral Al.

The pleochroism of the pyroxene bands at 3355, 3460, and 3535 cm^{-1} corresponds to an OH dipole orientation in the (100) plane close to the c axis. These bands may also be caused by OH dipoles present at O(2) positions, pointing in another direction. The pyroxene bands in orthopyroxene spectra usually have the strongest absorption in the γ polarization, as observed by Beran and Zemann (1986).

Amphibole bands

The sharp bands around 3675 cm^{-1} observed in most diopside-hedenbergite spectra and in some orthopyroxene spectra most likely are due to submicroscopic amphibole lamellae. These bands are prominent in the spec-

TABLE 5. Pleochroism of OH absorption bands in spectra of the India diopside (no. 2)

Section	E‖	[cm⁻¹] 3645	3535	3460	3355
(001)	a*	0.71	0.00	0.04	0.03
(001), (100)	b* = β**	1.00	0.36	0.28	0.27
(100)	c*	0.29	1.00	1.00	1.00
⊥c	a*	0.32	0.00	0.04	0.00
(010)	α**	0.59	0.44	0.28	0.30
(010)	γ**	0.00	0.89	0.96	0.62

Note: The intensities are normalized to the maximum absorbance observed for the individual bands.
 * a, b, and c are crystallographic directions.
 ** α, β, and γ are optical extinction directions.

TABLE 6. Estimation of amphibole lamellae in pyroxene by IR spectroscopy

No. sample	Geological environment	ΣA (3675)/ mm	Vol-ppm amphi-bole	amph : pyx
Diopsides				
3 Finland	metamorphic	0.602	1200	1:830
13 Ontario	high-grade metamorphic	0.520	1000	1:960
12 Norway	metamorphic	0.246	490	1:2000
41 Ontario	metamorphic	0.071	140	1:7000
4 New York	metamorphic	0.040	80	1:12000
10 Austria	metamorphic	0.022	44	1:23000
39 Sweden	metamorphic	0.019	38	1:26000
2 India	metamorphic	0.0093	19	1:54000
5 Madagascar	metamorphic	0.0072	14	1:69000
6 Switzerland	metamorphic	0.0060	13	1:83000
Orthopyroxenes				
31 Norway	megacryst	1.34	2700	1:370
36 Labrador	megacryst	1.20	2400	1:420
33 India	metamorphic?	0.093	186	1:5400
32 India	metamorphic?	0.0118	24	1:42000

Note: ΣA(3675)/mm denotes the summed absorbance for the three optical directions per mm. The amount of amphibole lamella was calculated from the summed absorbances assuming an absorbance of the OH bands of 500-mm thickness, derived from spectra of pure tremolite and actinolite (Skogby and Rossman, in preparation).

tra of two orthopyroxenes (nos. 36 and 31) previously shown to contain abundant submicroscopic amphibole lamellae (Veblen and Bish, 1988). Previously, Ingrin et al. (1989) reported a weak absorption band at 3675 cm⁻¹ in the spectrum of a diopside that contained submicroscopic amphibole lamellae.

The pleochroism of the sharp amphibole bands occurring around 3675 cm⁻¹ in many pyroxene spectra is somewhat different compared to the pleochroism we determined for OH bands in amphibole ($\alpha \sim \gamma$, $\beta = 0$ in clinopyroxenes, $\alpha > \gamma$, $\beta = 0$ in clinoamphiboles). Clinoamphibole lamellae in clinopyroxene usually are parallel to (010) and share crystallographic axes with the host structure (Veblen and Buseck, 1981). However, the extinction angles in (010) sections are different in monoclinic pyroxenes and amphiboles ($c \wedge Z = 38$–43° in diopside; $c \wedge Z = 14$–15° in tremolite). The polarization of the incident light will therefore be mixed in the submicroscopic amphibole lamellae, resulting in a more even intensity distribution in the α and γ directions.

Since amphiboles have very strong absorption bands (absorbance = ~500/mm thickness in tremolite-actinolite, Skogby and Rossman, in preparation), IR spectroscopy provides a very sensitive means of measuring concentrations of submicroscopic amphibole lamellae in pyroxenes. A summed thickness of amphibole lamellae in the pyroxene of less than 5 nm will be detectable under favorable conditions of sharp bands, as is the case for tremolite. An estimate of concentration of amphibole lamellae in our pyroxenes is in Table 6. Amphibole lamellae were detected in most metamorphic diopsides. Visible lamellae were not present in these samples. However, a few samples were too dark to offer a clear view of the beam path, so it is possible that visible amphibole lamellae escaped detection in these samples.

SUMMARY

All natural pyroxenes examined in this study, with the exception of a single meteoritic fassaite, contain detectable levels (>0.001 wt%) of structurally-bound hydroxyl. We conclude that OH-bearing pyroxenes are common in terrestrial geological environments.

The hydroxyl concentration varies as a function of geological environment, being greatest in samples of high pressure origin.

Initial OH contents of pyroxenes are probably a function of the thermodynamic activity of OH, subject to an upper limit imposed by the pyroxene crystal chemistry. Subsequent changes in external factors such as f_{O_2} and f_{H_2} may cause changes in the OH content.

The observed range of OH concentrations is presently estimated to be <0.001 to 0.12 wt% OH. This may be adjusted slightly as more accurate calibrations of the infrared technique are performed on a wider range of pyroxene compositions. Ranges of OH contents of orthopyroxenes and clinopyroxenes overlap considerably.

Infrared absorption spectra of the OH in pyroxenes comprise several bands (the pyroxene bands). In clinopyroxenes, the relative intensities of these bands correlate to some degree with composition.

Comparatively sharp absorptions at high wavenumber are due to OH in amphibole lamellae (the amphibole bands), which can be detected at levels equivalent to 5 unit cells in thickness. Amphibole lamellae have not been detected in mantle-derived pyroxenes in this study.

Although we have characterized the pleochroism of the OH absorptions and noted the influence of certain cations on band intensities, little is known about the actual site or sites of the OH groups in the pyroxene lattice. Furthermore, no direct substitutional mechanisms for the OH component have as yet been identified.

ACKNOWLEDGMENTS

REFERENCES CITED

Aines, R.D., and Rossman, G.R. (1984) Water content of mantle garnets. Geology, 12, 720–723.

Basu, A.R., Ongley, J.S., and MacGregor, I.D. (1986) Eclogites, pyroxene geotherm, and layered mantle convection. Science, 233, 1303–1305.

Beran, A. (1976) Messung des Ultrarot-Pleochroismus von Mineralen. XIV. Der Pleochroismus der OH-Streckfrequenz in Diopsid. Tschermaks Mineralogisches und Petrologisches Mitteilungen, 23, 79–85.

Beran, A., and Zemann, J. (1986) The pleochroism of a gem-quality enstatite in the region of the OH stretching frequency, with a stereochemical interpretation. Tschermaks Mineralogisches und Petrologisches Mitteilungen, 35, 19–25.

Boettcher, A.L., and O'Neil, J.R. (1980) Stable isotope, chemical, and petrographic studies of high-pressure amphiboles and micas: Evidence for metasomatism in the mantle source regions of alkali basalts and kimberlites. American Journal of Science, 280A, 594–621.

Burns, R.G., and Strens, R.G.J. (1966) Infrared study of the hydroxyl bands in clinoamphiboles. Science, 153, 890–892.

Cameron, M., and Papike, J.J. (1980) Crystal chemistry of silicate pyroxenes. In C.T. Prewitt, Ed., Pyroxenes. Mineralogical Society of America Reviews in Mineralogy, 7, 1–93.

Dixon, J.E., Clague, D.A., and Eissen, J.P. (1986) Gabbroic xenoliths and host ferrobasalt from the southern Juan de Fuca Ridge. Journal of Geophysical Research, 91B, 375–3820.

Dobson, P.F. (1986) The petrogenesis of the volcanic rocks of Chichi-Jima, Bonin Islands, Japan. Ph.D. thesis, Stanford University.

Duba, A., Dennison, M., Irving, A.J., Thornber, C.R., and Huebner, J.S. (1979) Electrical conductivity of aluminous orthopyroxene (abs.). Tenth Lunar and Planetary Science Conference, p. 318–319. Lunar and Planetary Institute, Houston, Texas.

Foit, F.F., Hooper, R.L., and Rosenberg, P.E. (1987) An unusual pyroxene, melilite, and iron oxide mineral assemblage in a coal-fire buchite from Buffalo, Wyoming. American Mineralogist, 72, 137–147.

Fortey, N.J., and Michie, U.McL. (1978) Aegirine of possible authigenic origin in Middle Devonian sediments in Caithness, Scotland. Mineralogical Magazine, 42, 439–442.

Hatton, C.J. (1978) The geochemistry and origin of xenoliths from the Roberts Victor Mine. Ph.D. thesis, University of Cape Town, South Africa.

Hazen, R.M., and Finger, L.W. (1977) Crystal structure and compositional variation of Angra dos Reis fassaite. Earth and Planetary Science Letters, 35, 357–362.

Ingrin, J., Latrous, K., Doukhan, J.C., and Doukhan, N. (1989) Water in diopside: An electron microscopy and infrared spectroscopy study. European Journal of Mineralogy, 1, 327–341.

Johnston, A.D., and Stout, J.H. (1984) A highly oxidized ferrian salite-, kennedyite-, forsterite-, and rhönite-bearing alkali gabbro from Kauai, Hawaii and its mantle xenoliths. American Mineralogist, 69, 57–68.

Keil, K., Prinz, M., Hlava, P.F., Gomes, C.B., Curvello, W.S., Wasserburg, G.J., Tera, F., Papanastassiou, D.A., Huneke, J.C., Murali, A.V., Scheinin, N.B., and Clayton, R.N. (1976) Progress by the consorts of Angra dos Reis. In Lunar Science VII, Lunar Science Institute, Houston, Texas, p. 443–445.

Miller, G.H., Rossman, G.R., and Harlow, G.E. (1987) The natural occurence of hydroxide in olivine. Physics and Chemistry of Minerals, 14, 461–472.

Paterson, M.S. (1982) The determination of hydroxyl by infrared absorption in quartz, silicate glasses and similar materials. Bulletin de Minéralogie, 105, 20–29.

Rossman, G.R., Rauch, F., Livi, R., Tombrello, T.A., Shi, C.R., and Zhou, Z.Y. (1988) Nuclear reaction analysis of hydrogen in almandine, pyrope and spessartite garnets. Neues Jahrbuch für Mineralogie Monatshefte, 172–178.

Skogby, H., and Rossman, G.R. (1989) OH in pyroxenes: An experimental study of incorporation mechanisms and stability. American Mineralogist, 74, 1059–1069.

Veblen, D.R., and Bish, D.L. (1988) TEM and X-ray study of orthopyroxene megacrysts: Microstructures and crystal chemistry. American Mineralogist, 73, 677–691.

Veblen, D.R., and Buseck, P.R. (1981) Hydrous pyriboles and sheet silicates in pyroxenes and uralites: Intergrown microstructures and reaction mechanisms. American Mineralogist, 66, 1107–1134.

Wilkins, R.W.T., and Sabine, W. (1973) Water content of some nominally anhydrous silicates. American Mineralogist, 58, 508–516.